Acta Ophthalmologica

Acta Ophthalmologica 2021

Defining inclusion criteria and endpoints for clinical trials: a prospective cross-sectional study in *CRB1*-associated retinal dystrophies

Mays Talib,[1] Mary J. van Schooneveld,[2,3] Jan Wijnholds,[1] Maria M. vanGenderen,[3] Nicoline E. Schalij-Delfos,[1] Herman E. Talsma,[1,3] Ralph J. Florijn,[4] Jacoline B. tenBrink,[4] Frans P.M. Cremers,[5] Alberta A.H.J. Thiadens,[6] L. Ingeborgh van denBorn,[7] Carel B. Hoyng,[8] Magda A. Meester-Smoor,[6] Arthur A. Bergen[4,9] and Camiel J.F. Boon[1,2]

[1]Department of Ophthalmology, Leiden University Medical Center, Leiden, The Netherlands
[2]Department of Ophthalmology, Amsterdam UMC, University of Amsterdam, Amsterdam, The Netherlands
[3]Bartiméus, Diagnostic Centre for complex visual disorders, Zeist, The Netherlands
[4]Department of Clinical Genetics, Amsterdam UMC, University of Amsterdam, Amsterdam, The Netherlands
[5]Department of Human Genetics and Donders Institute for Brain, Cognition and Behaviour, Radboud University Medical Center, Nijmegen, The Netherlands
[6]Department of Ophthalmology, Erasmus Medical Center, Rotterdam, The Netherlands
[7]Rotterdam Eye Hospital, Rotterdam, The Netherlands
[8]Department of Ophthalmology, Radboud University Medical Center, Nijmegen, The Netherlands
[9]The Netherlands Institute for Neuroscience (NIN-KNAW), Amsterdam, The Netherlands

ABSTRACT.

Purpose: **To investigate the retinal structure and function in patients with *CRB1*-associated retinal dystrophies (RD) and to explore potential clinical endpoints.**

Methods: **In this prospective cross-sectional study, 22 patients with genetically confirmed *CRB1*-RD (aged 6–74 years), and who had a decimal best-corrected visual acuity (BCVA) ≥ 0.05 at the last visit, were studied clinically with ETDRS BCVA, corneal topography, spectral-domain optical coherence tomography (SD-OCT), fundus autofluorescence, Goldmann visual field (VF), microperimetry, full-field electroretinography (ERG) and full-field stimulus testing (FST). Ten patients were from a genetic isolate (GI).**

Results: **Patients had retinitis pigmentosa (*n* = 19; GI and non-GI), cone-rod dystrophy (*n* = 2; GI) or macular dystrophy (*n* = 1; non-GI). Median age at first symptom onset was 3 years (range 0.8–49). Median decimal BCVA in the better and worse-seeing eye was 0.18 (range 0.05–0.83) and 0.08 (range light perception-0.72), respectively. Spectral-domain optical coherence tomography (SD-OCT) showed cystoid maculopathy in 8 subjects; inner retinal thickening (*n* = 20), a well-preserved (para)foveal outer retina (*n* = 7) or severe (para)foveal outer retinal atrophy (*n* = 14). All retinal layers were discernible in 13/21 patients (62%), with mild to moderate laminar disorganization in the others. Nanophthalmos was observed in 8 patients (36%). Full-field stimulus testing (FST) provided a subjective outcome measure for retinal sensitivity in eyes with (nearly) extinguished ERG amplitudes.**

Conclusions: **Despite the generally severe course of *CRB1*-RDs, symptom onset and central visual function are variable, even at advanced ages. Phenotypes may vary within the same family. Imaging and functional studies in a prospective longitudinal setting should clarify which endpoints may be most appropriate in a clinical trial.**

Key words: retina – retinal dystrophy – retinitis pigmentosa – gene therapy

The authors wish to acknowledge dr. Y.Y. Cheng (LUMC) for reviewing the corneal topography results.

Acta Ophthalmol.

doi: 10.1111/aos.14597

Introduction

Pathogenic variants in the *CRB1* gene are associated with a spectrum of retinal dystrophies (RD). Each RD can be distinguished clinically depending on the age at symptom onset, electrophysiological findings and other phenotypic features. *CRB1* mutations cause up to 17% of cases of Leber congenital amaurosis (LCA) and up to 9% of cases of autosomal recessive nonsyndromic retinitis pigmentosa (RP) (Vallespin et al. 2007; Corton et al. 2013; Sánchez-Alcudia et al. 2014), as well as rare cases of isolated maculopathy (Tsang et al. 2014; Mucciolo et al. 2018). *CRB1*-associated LCA causes severe visual impairment or blindness from infancy, and *CRB1*-RP usually has an early onset of symptoms such as nyctalopia and visual field restriction, although cases of a later symptom onset and/or relative preservation of visual acuity in *CRB1*-RP have also been described (Mathijssen et al. 2017; Talib et al. 2017). While most clinical studies of the human *CRB1*-associated phenotype have been case series or small cohorts (Jalkh et al. 2014; Khan et al. 2014; Tsang et al. 2014; Yang et al. 2014; Morarji et al. 2016; Vincent et al. 2016), recent studies in larger populations have shown that half of *CRB1*-RP patients are expected to reach low vision or blindness by the ages of 18 and 44, respectively (Mathijssen et al. 2017; Talib et al. 2017). Reports on associated features in *CRB1*-RP or LCA, such as keratoconus, have shown a variable prevalence (den Hollander et al. 1999; Lotery et al. 2001a; Lotery et al. 2001b; Bernal et al. 2003; Galvin et al. 2005; McKibbin et al. 2010; Jalkh et al. 2014). As protein CRB1 is crucial for the integrity of the retinal structure, *CRB1*-associated RDs have shown an association with variable degrees of disorganization of the retinal laminar structure (van de Pavert et al. 2004). While no effective and approved treatment for *CRB1*-associated retinopathies is currently available, subretinal adeno-associated virus (AAV)-mediated *CRB1-CRB2* gene augmentation therapy has shown functional and structural rescue in murine models of *CRB1*-associated LCA and RP (Pellissier et al. 2015). As human *CRB1* gene therapy is under development (Quinn et al. 2017), defining an optimal window of therapeutic opportunity and clinical endpoints for a *CRB1* gene therapy trial is essential. In such trials, measures that are time-dependent and can still remain stable in certain decades of life, such as visual acuity (Talib et al. 2017), may need to be complemented with other, potentially more sensitive functional or structural outcome measures. These additional outcome measures have not yet been elucidated, as an inevitable limitation of retrospective studies is the limited availability of extensive imaging and functional examinations, as well as the unstandardized design. The aim of the present study was to extensively investigate the retinal structure and function in patients with *CRB1*-RDs in a clinical study of prospectively enrolled patients and to study the correlation between structural and functional parameters in order to assess potentially sensitive efficacy endpoints for a future gene therapy trial.

Materials and methods

Human subjects

This is a nationwide collaborative study, based on the Delleman archive for hereditary eye diseases at the Amsterdam UMC (University of Amsterdam) and the RD5000 consortium, the Dutch national consortium for the registry of patients with retinal dystrophies. Inclusion criteria for this prospective, cross-sectional study were (1) the presence of two confirmed pathogenic variants in the *CRB1* gene (class 4 or 5), (2) a decimal BCVA of $\geq$0.05 in the better-seeing eye at the last available clinical examination, which (3) should not have been >20 years prior to enrolment in this study. Of the 63 identified *CRB1*-RD patients in the Netherlands, 22 could be included based on these inclusion criteria (Fig. S1). In one patient (ID-9), the worse-seeing eye had light perception vision, and not all tests could be performed in the worse-seeing eye. The cohort included patients from a Dutch genetic isolate, that is a consanguineous pedigree described earlier (van den Born et al. 1994). Patients and/or their parents signed informed consent. This study was approved by the Medical Ethics Committee of the Erasmus Medical Center, as it was performed in the framework of the RD5000 consortium (van Huet et al. 2014), and by the local review board of the Leiden University Medical Center (LUMC), and complied with the tenets of the Declarations of Helsinki.

Ophthalmological assessment

A detailed medical and ophthalmological history was recorded in all subjects. Patients were surveyed on the history of their symptoms, the presence of photopsia, and in the case of photopsia, where in the visual field these were located (full field, periphery or central areas). Participants underwent a complete ophthalmological examination, including best-corrected visual acuity (BCVA) measurements with the Early Treatment of Diabetic Retinopathy Study (ETDRS) ESV-3000 chart by Precision Vision (Ferris et al. 1982; Ferris & Bailey 1996), slit-lamp biomicroscopy, fundoscopy and Goldmann kinetic perimetry. Corneal topography was evaluated using the 4-map refractive report and the Belin/Ambrósio Enhanced Ectasia report (Oculus Optikgerate GmbH, Wetzlar, Germany). Biometry was performed (Eye-Suite™ IOL, Haag-Streit Diagnostics) to measure eye axis length and anterior chamber depth. Macular threshold sensitivities were measured under mesopic conditions with Macular Integrity Assessment microperimetry (MAIA, Centervue, Padova, Italy) in 20 patients, as the youngest two patients (aged 6 and 9 years) could not complete the procedure. To minimize a learning effect, each eye was tested using the '4-levels-fixed' protocol, which familiarizes the patient to the test, followed by testing with the '4-2 staircase strategy', projected on a 10-2 Cartesian grid (37 points covering the central 10°). The latter was used to evaluate the macular sensitivity (average threshold) and fixation stability (bivariate contour ellipse area; BCEA). The 95% or 65% BCEA indicates the ellipse area that comprises 95% or 65%, respectively, of the fixation points used by the patients during the test. Thus, a smaller area indicates a more stable fixation. Seven-field colour fundus photographs were obtained (Topcon TRC-50DX, Topcon Medical Systems, Inc. Oakland, NJ, USA). Spectral-domain optical coherence tomography (SD-OCT; Spectralis, Heidelberg Engineering, Heidelberg,

Germany) of the macula and optic disc was performed in 21 patients, but could not be reliably performed in the 6-year-old patient. Segmentation of SD-OCT images was performed with the integrated automatic segmentation Spectralis software, and errors in the segmentation were manually corrected. Thickness of the photoreceptor–retinal pigment epithelium complex (PR + RPE) was measured as the distance from the external limiting membrane (ELM) to the basal membrane, based on methods used earlier (van Huet et al. 2015). The horizontal width of detectable and uninterrupted (even if attenuated) ellipsoid zone (EZ) was measured drawing a line parallel to the retinal pigment epithelium (RPE), starting at the fovea. In patients where the EZ signal became indistinguishable from other hyperreflective outer retinal signals and could no longer be differentiated from the ELM or interdigitation zone, the horizontal width of detectable hyperreflective outer retinal band was measured. The laminar organization of the retina, that is the retinal alignment into distinct layers, was assessed and categorized (Fig. S2). In 20 patients, 488 nm wavelength fundus autofluorescence (FAF; Spectralis, Heidelberg Engineering, Heidelberg) was performed, which could not be reliably performed in the two youngest patients (aged 6 and 9 years). The fovea was defined as the central 5°, the parafovea as the following circumferential 3° around the fovea and the perifovea or peripheral macula as the circumferential 10° around the parafovea.

Pupil dilation protocol

Initially, all pupils were dilated using phenylephrine 2.5% and tropicamide 1%. After the occurrence of acute angle-closure glaucoma in one patient during mydriatic dark adaptation with tropicamide only (patient ID-15, the 9th consecutive patient who participated), the pupil dilation protocol was revised: only patients with an anterior chamber depth ≥ grade 2, as graded with the pen torch method and Van Herick's technique, received phenylephrine 2.5% and tropicamide 1%. In patients with an anterior chamber depth of grade 2, pupils were dilated using only tropicamide 1%. The pupils of one patient (patient ID-4, the 10th consecutive patient) with an anterior chamber depth of grade 1, and a family history of acute angle-closure glaucoma in relatives with *CRB1*-RP, were not dilated.

Electrophysiological testing

Full-field electroretinography (ERG) was performed according to an extended protocol, which incorporated the International Society for Clinical Electrophysiology Standards (McCulloch et al. 2015). All ERG responses were recorded using Dawson Trick Litzkow (DTL) fibre electrodes with the Espion ColorDome™ and console (Diagnosys LLC, Cambridge, UK). The set-up and reference values of the Rotterdam Eye Hospital (Rotterdam, The Netherlands) and Bartiméus (Zeist, The Netherlands) were used. For an RP diagnosis, attenuation of the dark-adapted responses had to be more severe than attenuation of the light-adapted responses. The reverse was the case for a cone-rod dystrophy (CORD) diagnosis. In the case of nondetectable responses, the diagnosis was made based on the clinical evidence (e.g. fundoscopy). For an isolated macular dystrophy diagnosis, the full-field ERG should display no panretinal dysfunction of dark- or light-adapted responses. Full-field stimulus testing (FST) was successfully performed in 15 subjects (28 eyes) with the Espion ColorDome™ LED full-field stimulator (Diagnosys LLC, Lowell, MA, USA) using methods described previously (Roman et al. 2007; Klein & Birch 2009; Collison et al. 2014), after dark adaptation of ≥30 min, and using white red, and blue stimuli, each lasting 4 milliseconds. Each eye was tested separately, and the fellow eye was patched. The reference luminance (0 dB) was set at 0.1 cd.s/m^2. Sensitivity thresholds were determined three times for each colour, and the three trials were averaged to determine the final thresholds. General sensitivity thresholds were determined using the white stimuli. Chromatic sensitivities were used to determine whether these responses were rod-mediated (blue-red difference of >22 dB), cone-mediated (blue-red difference of <3 dB) or mixed rod- and-cone- mediated (blue-red difference between 3 and 22 dB). Based on earlier studies (Roman et al. 2005; Roman et al. 2007), and correcting for differences in reference luminance, the normal FST threshold for white stimuli was determined at −53 dB and should be rod-mediated.

Statistical analysis

Data were analysed using SPSS version 23.0 (IBM Corp, Armonk, NY, USA). Normality was tested using the normal probability plot and quantile–quantile plot, and the Shapiro–Wilk test. Normally distributed data were presented with means and standard deviations (SD). Non-normally distributed data were presented with medians and interquartile ranges (IQR). Goldmann visual field areas of the V4e target were digitized and converted to seeing retinal areas in mm^2 using a method described by Dagnelie (Dagnelie 1990). Visual field areas were classified as large (>250 mm^2), intermediate (25–250 mm^2) or small (<25 mm^2), based on an earlier study (Koenekoop et al. 2014). Medians were compared using the Mann–Whitney *U*-test. The correlation between visual function parameters (BCVA, macular sensitivity on microperimetry, V4e and I4e visual field extent) and biomarkers on retinal imaging was tested with Spearman's correlation testing. Visual impairment, based on the BCVA, was categorized as defined by the World Health Organization: mild or no visual impairment (BCVA ≥ 0.3), low vision (BCVA < 0.3 and ≥0.1), severe visual impairment (BCVA < 0.1 and ≥0.05) and blindness (BCVA < 0.05). For statistical analysis, ETDRS BCVA was converted to the logarithm of the minimal angle of resolution (logMAR).

Results

Twenty-two patients with *CRB1*-RD were included, from 12 families. Table 1 shows the baseline clinical characteristics. Ten patients (45%) were from the genetic isolate. The median age at examination was 25 years (IQR 20; range 6–74) and did not differ significantly between patients from within and from outside the genetic isolate (p = 0.57). Nine patients (41%) were male (aged 6–74), and 13 (59%) were female (aged 9–38). Based on current and previous ERG examinations, 19 patients (86%) were diagnosed with RP, 2 patients (9%; 1

Table 1. Demographics and baseline findings in ophthalmological examination in patients with *CRB1*-associated retinal dystrophies.

ID/Sex/ Family	Age (y)	Age (y) at onset 1st symptom	BCVA (ETDRS letters [decimal Snellen])		SER (D)**	ffERG	Central horizontal VF diameter (°)		Total seeing retinal area V4e (mm^2)	
			OD	OS			OD	OS	OD	OS
1/M/GI*	29	6	34 (0.10)	61 (0.33)	+0.56	ND	27	30	154.6	158.1
2/F/GI	13	1.5	39 (0.12)	40 (0.13)	+3.06	ND‡	24	24	33.9	36.9
3/F/GI	16	1	52 (0.20)	56 (0.25)	+0.56	RCD	22	28	119.7	160.7
4/F/GI	38	<1	23 (0.06)	40 (0.13)	+1.00	ND‡	25	24	34.1	38.8
5/M/GI	41	2	40 (0.13)	13 (0.04)	+3.88	ND	19	19	90.5	74.9
6/F/GI	11	3	56 (0.26)	64 (0.38)	+3.19	MR	29	105	260.9	296.2
7/F/GI	9	2	19 (0.05)	19 (0.05)	+6.31		30	21	240.0	183.9
8/F/GI	10	3	31 (0.08)	22 (0.05)	+7.06	MR	150	45	624.4	450.4
9/F/GI	28	8	5 (0.03)	35 (0.10)	+5.75	ND	25	21	164.3	185.6
10/M/GI	39	34-35	78 (0.72)	78 (0.72)	+2.5	CORD	150	150	746.9	711.8
11/M	31	7-8	70 (0.50)	81 (0.83)	+1.00	MR	62	125	278.9	370.3
12/F	26	9	53 (0.23)	61 (0.33)	+1.44	ND	51	110	279.1	345.8
13/M	21	2	12 (0.03)	30 (0.08)	+2.56	ND‡	70	53	215.0	189.9
14/F	24	2	52 (0.22)	20 (0.05)	+5.25	ND‡	36	26	79.1	85.5
15/F	31	1	41 (0.13)	42 (0.14)	+4.75	ND‡	22	24	175.2	146.24
16/M	6	1-2	11 (0.03)	25 (0.06)	+3.38	NP	72	62	231.9	123.19
17/M	23	12	63 (0.36)	27 (0.07)	***	RCD	101	20	553.6	348.1
18/F	12	3	40 (0.13)	19 (0.05)	+5.00	ND	15	16	135.0	116.8
19/M	53	17	52 (0.22)	0 (NLP)†	***	ND	18	0	33.4	0
20/M	74	49	75 (0.63)	58 (0.29)	***	ND	20	19	17.9	22.4
21/F	31	4	30 (0.08)	31 (0.08)	+0.88	CORD	65	25	703.0	717.3
22/F	24	11–12	66 (0.41)	42 (0.14)	−5.75	Normal	148	148	723.7	754.8

BCVA = best-corrected visual acuity, CORD = cone-rod dystrophy, ETDRS = Early Treatment of Diabetic Retinopathy Study, ERG = full-field electroretinography, GI = genetic isolate, MR = minimal response, ND = no detectable responses, NP = not performed (patient did not tolerate the electrodes), SER = spherical equivalent of the refractive error, VF = (Goldmann) visual field.

* These patients were also included in the previous retrospective cohort. One patient (ID 1) underwent electrophysiological testing with a different device (MetroVision) prior to the acquisition of the Diagnosys device.

** Averaged between eyes.

*** These patients had undergone cataract surgery in one (patient 17) or both (patients 19–20) eyes, and these refractive error measurements are postoperative. Preoperatively, the SER was −0.5 D and −1.875 D in patients 19 and 20, respectively.

† Patient 19 reported no light perception in OS during BCVA measurement, but after dark adaptation in mydriasis in preparation for electrophysiological examination, he could perceive white, red and blue stimuli with OS.

‡ Scotopic and photopic responses had been nondetectable in ERG examination performed prior to this study.

from the genetic isolate) had a cone-rod dystrophy, and 1 patient (5%) had a macular dystrophy. Table S1 shows the genetic characteristics, including the novel *CRB1* variant p.(Phe978Ser) in a patient with severe RP (ID-16), and the homozygous p.(Ile167_Gly169-del) variant in the macular dystrophy patient (ID-22). Nineteen patients (86%) were of Dutch Caucasian descent, 2 were of North African origin (9%), and 1 patient was of Caribbean descent (Dutch Antilles; 5%).

Onset and visual acuity

The median self-reported or parent-reported age at symptom onset was 3 years in the RP group (IQR 6.5 years; range 9 months-49 years) and 11 years in patients with a cone-rod or macular dystrophy (range 4–34 years). In the RP group, the first-experienced symptoms, as noticed either by the patient or by the parents, were visual field loss (8/19; 42%), nyctalopia (5/19; 26%), central vision loss (4/19; 21%) or nystagmus (2/19; 11%). In RP patients ID-6 and ID-17, the initial erroneous diagnosis was intermediate uveitis, based on central vision loss, CME and vitreous cells, all of which preceded pigmentary fundus changes. After 1 and 4 years, respectively, the correct diagnosis of RP was established based on full-field ERG responses, and the course towards the correct diagnosis has been described previously (Hettinga et al. 2016). In the three patients with cone-rod or macular dystrophy, the first symptom was subjective central vision loss. There was no statistically significant difference in median age at symptom onset between patients from within and from outside the genetic isolate ($p = 0.22$). Photopsia were reported by 13 patients (59%) in areas of decreased/no vision ($n = 3$), areas of good vision ($n = 2$) or in both ($n = 8$).

The median decimal BCVA in the better-seeing eye was 0.18 (0.05–0.83), and 0.08 in the worse-seeing eye (range light perception vision-0.72), with a moderate symmetry between the right and left eye (Spearman's rho = 0.467; $p < 0.028$). Best-corrected visual acuity (BCVA) in the better-seeing eye did not significantly differ between patients from within or from outside the genetic isolate ($p = 0.53$), but was significantly better in older patients (Spearman's rho = 0.435; $p = 0.04$; Fig. 1).

Ocular and fundus features

The median spherical equivalent of the refractive error, as averaged between both eyes, was +3.1D (IQR 4.0, range −5.75D to +7.06). The median eye axis length was 20.7 mm, with a median anterior chamber depth of 2.8 mm.

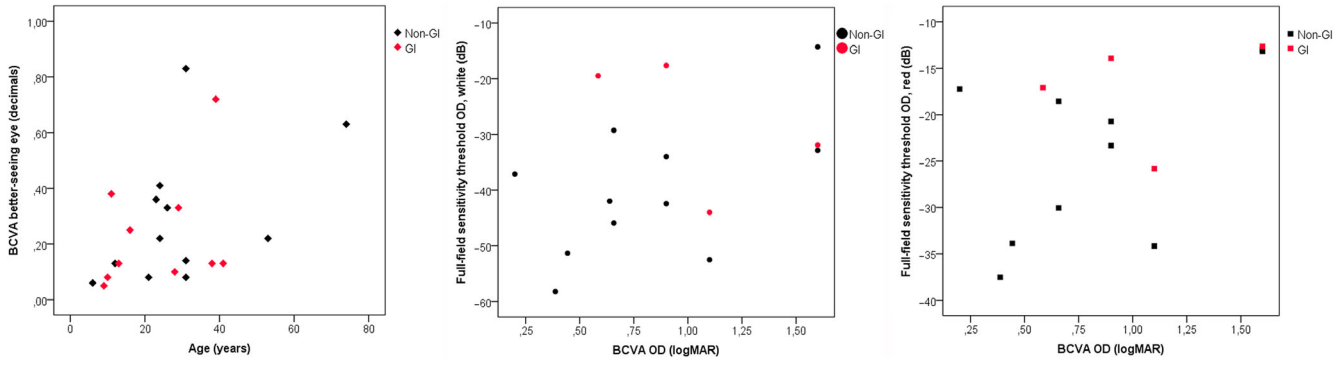

Fig. 1. Visual function in patients with *CRB1*-associated retinal dystrophies. Patients from the genetic isolate (GI) are indicated in red, and the other patients are indicated in black. The left panel shows the best-corrected visual acuity (BCVA) as plotted against age. A higher BCVA is seen in older patients (Spearman's rho = 0.435; p = 0.043), possibly because the inclusion criterion of a BCVA ≥ 0.05 allows only for the inclusion of either young patients with a severe phenotype, or patients with a mild phenotype, who have a wider window of opportunity for study inclusion. The middle panel shows the full-field sensitivity threshold to white light (in dB), plotted against BCVA. Although sensitivity thresholds to white stimuli appeared better (signified by lower dB) in patients with a better BCVA, this trend was not significant (Spearman's rho = 0.344; p = 0.209). The right panel shows full-field sensitivity threshold to red light (dB), plotted against BCVA. Again, sensitivity thresholds to red stimuli appeared lower in those with a higher BCVA. This trend seemed more strongly apparent for the red stimuli than for the white stimuli, but was still not significant (Spearman's rho = 0.493; p = 0.073).

Nanophthalmos (axial length < 20.5 mm) was observed in eight patients (36%). Cataracts, defined as significant opacification of the lens, were observed in 11 eyes of six patients (27%), and 3 patients (14%) were pseudophakic in at least one eye. Corneal topography could be reliably performed in 20 patients and revealed a mild to moderate with-the-rule astigmatism in 15 patients (75%), a mild oblique astigmatism in one patient (15%) and a mild against-the-rule astigmatism in one patient (5%). One patient had a mild forme fruste keratoconus (patient ID-21), and 3 more had a corneal topography suspicious of a mild forme fruste keratoconus, which would need to be confirmed upon follow-up (patients ID-11; ID-15; ID-22). Vitreous abnormalities in 14 patients (63%) included cells (n = 12), veils (n = 3), and asteroid hyalosis (n = 1). Two patients had undergone a pars plana vitrectomy with inner limiting membrane peeling due to cystoid macular oedema (patients ID-17 and ID-19) or the presumably erroneous diagnosis of intermediate uveitis, which was unresponsive to lengthy immunosuppressive treatment. Fundus features were variable, even within the genetic isolate (Figs 2 and 3), but all patients had macular alterations of the retinal pigment epithelium, and 16/22 patients (73%), aged 10–53, had atrophic changes of the macula. Drusen within or hamartomas around the optic nerve head were seen in seven patients (32%), and were observed more frequently in patients from the genetic isolate (6/10 versus 1/12; p = 0.02). Fine yellow punctate spots in the peripheral retina were observed in eight patients (36%), all with RP, and were more prominent in the nasal periphery (Fig. 2). Intraretinal pigment migrations were present in 21/22 patients with RP or CORD (95%; aged 6–74 years) and not in the patient with a macular dystrophy. These pigment migrations were bone-spicule-like (n = 5), nummular (n = 1) or a combination of both (n = 15). Preservation of the para-arteriolar retinal pigment epithelium (PPRPE) was observed in 3/22 patients (14%). Retinal vascular changes included a unilateral preretinal haemorrhage of unknown origin in patient ID-8, aged 10, and parapapillary hard exudates in patient ID-5 (Fig. 2), whose affected younger sister (not included in the current study) had unilateral Coats-like exudates. Furthermore, vascular attenuation was featured in 18/22 patients (82%), but was absent in the macular dystrophy patient (age 24) and in the youngest RP patients (aged 6–10), considerably mild in the adolescent RP patients (aged 12–16), and was mild in the CORD patients (aged 31 and 39).

Perimetry

Visual field areas, averaged between right and left eyes, were large in 8/22 patients (36%), intermediate in 12/22 (55%) and small in 2/22 patients (9%). Visual field areas did not significantly correlate to age (p = 0.25 and p = 0.61 for the V4e and I4e isopter).

Microperimetry could not be reliably performed in the 2 youngest patients and was challenging to perform in patients with severe visual impairment: between the test run using the 4-levels-fixed strategy, and the examination using the 4-2 strategy, the preferred retinal locus had shifted in nine eyes of six patients (three eyes with low vision; five eyes with severe visual impairment; and one blind eye). The average threshold of the macular sensitivity on microperimetry was 8.0 dB (SD 6.9; range 0.2–25.3; normal range 26.0–36.0 dB; Table S2). Macular sensitivity was significantly lower in eyes with decreased fixation stability, as indicated by a higher BCEA 95%, averaged between right and left eyes (Spearman's rho = −0.478; p = 0.045). Inter-eye symmetry was very high for the average threshold of the macular sensitivity (Spearman's rho = 0.821; p < 0.0001) and V4e visual field area (Spearman's rho = 0.955; p < 0.00001; Fig. S3). There was no significant difference between patients from within and from outside the genetic isolate in visual field areas for the V4e (p = 0.74) and I4e (p = 0.60), or macular sensitivity (p = 0.66).

Rod and cone function

Dark-and light-adapted full-field ERG responses were nondetectable in 12/20

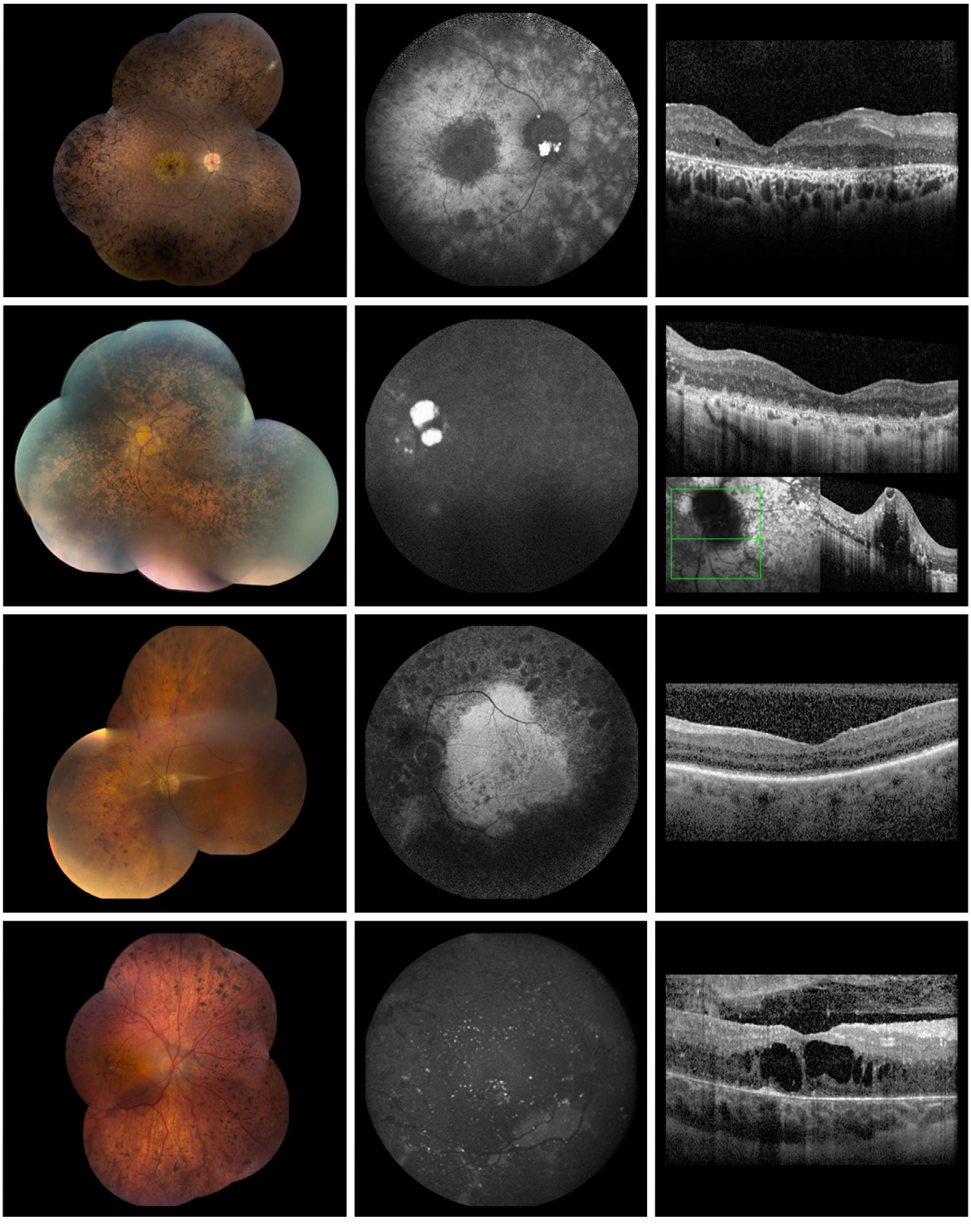

Fig. 2. Multimodal imaging in patients with *CRB1*-associated retinitis pigmentosa (RP). The top row shows the right eye of patient ID-9, a 28-year-old female patient from the genetic isolate (GI) with a decimal best-corrected visual acuity (BCVA) of 0.03, whose fundus (left panel) showed the typical RP-associated changes of bone-spicule-like pigmentation in the (mid)periphery, vascular attenuation and optic disc pallor, but also large parapapillary hamartomas, atrophy of the retina and retinal pigment epithelium (RPE) in the posterior pole, and white flecks resembling reticular pseudodrusen throughout the retina, associated with outer retinal atrophy. Fundus autofluorescence (FAF; middle panel) showed large meshwork-like areas of hypo-autofluorescence in the midperiphery and central macula, with relatively spared perimacular autofluorescence. Spectral-domain

optical coherence tomography (SD-OCT; right panel) showed inner retinal thickening, outer retinal atrophy, (para)foveal granular remnants of the hyperreflective outer retinal bands, but no laminar disorganization. The second row shows the left eye of patient ID-5, a 41-year-old male patient from the GI (BCVA 0.04). The fundus (left panel) was profoundly atrophic with dense intraretinal pigmentation, parapapillary hamartomas, fine drusenoid deposits in the nasal periphery, and parapapillary hard exudates that indicate a vascular disease component. Fundus autofluorescence (FAF) (middle panel) showed a near absence of autofluorescence. Spectral-domain optical coherence tomography (SD-OCT) (right panel) showed mild laminar disorganization, a relatively thickened inner retina, outer retinal atrophy with a severely disrupted ellipsoid zone (EZ) and a barely identifiable external limiting membrane (ELM), and small hyperreflective foci mainly in the inner nuclear layer and ganglion cell layer. Spectral-domain optical coherence tomography (SD-OCT) of the optic disc (right panel) showed the hamartoma, and dense hyperreflective foci colocalizing with the parapapillary exudates, but no source of the exudation. The third row shows the left eye of patient ID-20, a 74-year-old male patient from outside the GI (BCVA 0.29), which showed typical RP-associated changes (left panel), along with mild macular RPE alterations. Fundus autofluorescence (FAF) (middle panel) was relatively preserved in the posterior pole with scattered round hypo-autofluorescent lesions and severe hypo-autofluorescence outside the vascular arcades. Spectral-domain optical coherence tomography (SD-OCT) (right panel) showed a relatively preserved outer nuclear layer, ELM and EZ. The fourth row shows the right eye of patient ID-8, a 10-year-old female patient from the GI (BCVA 0.08), whose fundus (left panel) showed bone-spicule-like and round intraretinal pigmentation, atrophy in the posterior pole, a preretinal bleeding under the central macula, some preservation of the peri-arteriolar RPE in the inferior and superior periphery, and limited fine drusenoid deposits, mostly in the nasal midperiphery. Fundus autofluorescence (FAF) (middle panel) showed severely decreased autofluorescence, with some relative preservation along the inferior vascular arcade, and sharply circumscribed hyperautofluorescent speckles, which may be photoreceptor debris containing lipofuscin precursors. These speckles were also found in patient ID-18. Spectral-domain optical coherence tomography (SD-OCT) (right panel) showed cystoid macular oedema, a thickened inner retina and a severely atrophic ELM and EZ, with scattered para- and perifoveal remnants.

patients (60%; aged 12–73; Table 1). Dark-adapted FST thresholds were obtained in 15 subjects (28 eyes for white stimulus; 27 eyes for red and blue stimuli), 9 of whom had no detectable dark- or light-adapted responses on ERG, and 2 more with nearly nondetectable responses. General FST sensitivity for the white stimulus, averaged between eyes, ranged between −56.2 and −13.4 dB (mean −36.1; SD 12.7). Sensitivity thresholds were mediated by a mixed rod-cone response (17/27 eyes; 63%) or were rod-mediated (10/27 eyes; 37%, which included the four eyes of two patients with cone-rod or macular dystrophy). The FST thresholds for red stimuli, which are typically mostly cone-mediated, were not significantly associated with biomarkers on SD-OCT (Table 2). The median inter-eye difference in FST threshold was 4.0 dB (IQR 7.8; range 0.24–14.0). For each eye, each threshold was tested three times. The results of the three intra-ocular measurements were generally consistent (median largest within-visit difference between each pair of measurements of the white stimulus threshold was 2.07 dB; IQR 1.84; range 0.31–8.62).

Imaging

Spectral-domain optical coherence tomography (SD-OCT) showed bilateral cystoid macular oedema (CME) in the inner nuclear layer (INL) of 8/21 patients (38%), 2 of whom also had CME in the ONL. Patient ID-11 also had macular retinoschisis with splitting in the outer plexiform layer. Patients with CME seemed younger (mean age 21.1; SD 10.4; range 10–39) than those without CME (mean age 31.9; SD 17.1; range 9–74), although this difference was not statistically significant ($p = 0.13$). However, decimal BCVA was higher in patients with CME (median 0.25; IQR 0.43; range 0.07–0.72) than in those without CME (median 0.10; IQR 0.10; range 0.05–0.46; $p = 0.03$). Cystoid macular oedema (CME) was mostly refractory to treatment (Table S3). A mild epiretinal membrane was observed in nine patients (41%; bilateral in 6/9), and patient ID-11 had a lamellar pseudohole in one eye. The retinal laminar organization was relatively disorganized in 8/21 patients (38%), had a coarse aspect but no disorganization in 8/21 patients (38%) and was normal in 5/21 patients (24%; Fig. S2). No outer retinal tubulations were observed.

The outer retinal layers at the (para) fovea, that is outer nuclear layer and hyperreflective outer retinal bands (external limiting membrane and ellipsoid), showed moderate to severe disintegration in 14/21 patients (67%) aged 13–53, with a near absence of these layers in three of these patients, but only mild thinning in 7/21 patients (33%) aged 9–74. In the more peripheral macula, the outer retinal layers were nearly absent in 5/21 (24%), markedly attenuated in 10/21 patients (48%) and only mild thinning in 6/21 patients (29%). The general pattern consisted of more severe outer retinal attenuation in the peripheral macula with relative foveal remnants of the outer retina, with the exception of patients ID-10, ID-21 and ID-22, who had more intact outer retina in the peripheral macula. Figure S4 shows the horizontal width of detectable uninterrupted ellipsoid zone band for each patient. No significant correlations were found between foveal retinal thickness or the horizontal width of visible ellipsoid zone and visual function parameters after correction for multiple testing, but the PR + RPE thickness correlated significantly with BCVA ($p = 0.001$; Table 2). Mild to severe thickening of the inner retinal layers was observed in 20/21 patients (95%), which was not correlated to thinning of the outer retina and RPE (Fig. S4). Fundus autofluorescence (FAF) images showed intra- and interfamilial variability in the degree of retinal pigment epithelium preservation (Fig. 2 and 3), ranging from generalized severely decreased or (nearly) absent autofluorescence ($n = 4$; aged 13–41 years), to relative preservation of autofluorescence in the posterior pole or around the vascular arcade ($n = 10$; aged 11–74 years), to a generally normal or mildly hypo-autofluorescent retina with zones of granular or bone-spicule-like hypo-autofluorescence ($n = 3$; aged 16–31 years). Patients with CORD had different patterns of macular hypo-autofluorescence. A hyperautofluorescent ring was only observed in patient ID-22 with a macular dystrophy.

Discussion

In this prospective cross-sectional study, we performed detailed clinical examinations in patients with *CRB1*-associated RDs, demonstrating a wide

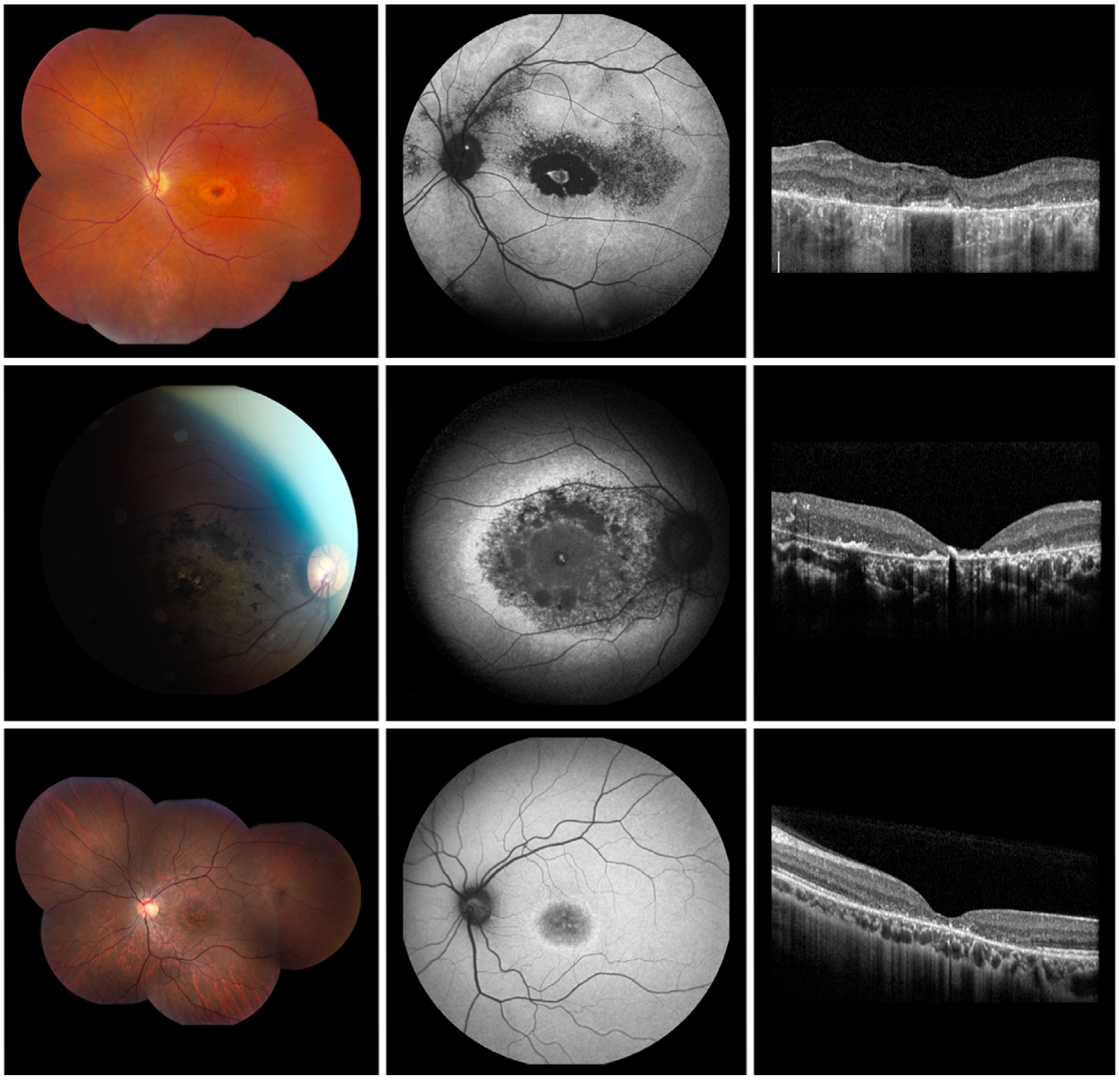

Fig. 3. Multimodal imaging in patients with *CRB1*-associated cone-rod or macular dystrophy. The top row shows the left eye of patient ID-10, a 39-year-old male patient from the genetic isolate with cone-rod dystrophy (CORD) and a decimal best-corrected visual acuity (BCVA) of 0.72, whose fundus (left panel) showed mild parapapillary atrophy, mild vascular attenuation and stretching in the periphery, atrophy of the retina and retinal pigment epithelium (RPE) in a parafoveal ring around a hyperpigmented fovea, along with RPE alterations in the temporal posterior pole and regional chorioretinal atrophy with limited bone-spicule-like pigmentation in the inferior periphery. Fundus autofluorescence (FAF; middle panel) showed a small optic disc druse, a parafoveal ring of absent autofluorescence, surrounded by dense granular hypo-autofluorescence with scattered hyperautofluorescent lesions mainly in the superior and temporal posterior pole. These granular changes are also visible along the superior vascular arcade, and in the nasal and inferior midperiphery. Spectral-domain optical coherence tomography (SD-OCT) (right panel) showed a thickened inner retina, a severely attenuated outer nuclear layer (ONL) and relative sparing of the hyperreflective outer retinal bands in the fovea and to a lesser extent in the peripheral macula, with severe disruption in the parafoveal region. The second row shows the right eye of patient ID-21, a 31-year-old female patient of Caribbean origin (Dutch Antilles) with CORD (BCVA 0.08), which showed (left panel) relative preservation of the optic disc colour and vascular calibre, but atrophy of the retina and RPE in the posterior pole, with large round and bone-spicule-like pigmentations that partially fused, and some bright RPE alterations in the central macula. The (mid)peripheral retina (not shown here) was well-preserved. Fundus autofluorescence (FAF) (middle panel) showed a large parafoveal area of even hypo-autofluorescence around a foveal hyperautofluorescent lesion, surrounded by patches of absent autofluorescence and granular hypo-autofluorescence. A broad and mildly hyperautofluorescent ring encircled this region of hypo-autofluorescent changes. Spectral-domain optical coherence tomography (SD-OCT) (right panel) showed a mildly thickened inner retina and a profoundly atrophic outer retina, and a relatively preserved laminar structure. The third row shows the left eye of patient ID-22, a 24-year-old female patient of North African origin with macular dystrophy (BCVA 0.14), whose fundus (left panel) showed a mild temporal pallor of the optic disc, atrophic macular RPE alterations with visible choroid, and an otherwise normal fundus. Fundus autofluorescence (FAF) (middle panel) showed hypo-autofluorescent changes in the central macula, encircled by a hyperautofluorescent ring, surrounded by normo-autofluorescent retina. The granular hypo-autofluorescent changes corresponded with severe ONL atrophy, and disruptions of the external limiting membrane and the ellipsoid zone on SD-OCT (right panel).

Table 2. Structure and function correlations in *CRB1*-associated retinopathies.

	Foveal EZ width		PR + RPE thickness		CRT**	
Visual function parameter	Spearman's rho	p-value	Spearman's rho	p-value	Spearman's rho	p-value
BCVA (logMAR)	−0.581	0.007	0.656	**0.001**	0.424	0.070
Average threshold for MS (dB)	0.433	0.064	0.489	0.029	0.449	0.062
Central sensitivity* (dB)	0.506	0.027	0.502	0.024	0.424	0.080
BCEA 63%	−0.385	0.127	−0.453	0.059	−0.159	0.557
BCEA 95%	−0.385	0.127	−0.453	0.059	−0.159	0.557
Seeing retinal area V4e	−0.095	0.691	−0.226	0.324	-0.144	0.557
Seeing retinal area I4e	0.123	0.605	0.097	0.674	0.181	0.457
FST thresholds white light (dB)	0.319	0.289	0.319	0.267	0.140	0.665
FST thresholds red light (dB)	0.396	0.181	0.358	0.208	0.259	0.417

Values for all parameters were averaged between the right and left eye for each patient. When data were available for one eye only, the data for that eye were used. For measurement of the EZ width, values were measured from the central fovea. If the EZ band was interrupted and continued in the peripheral macula, this peripheral EZ was not included in the EZ width. Significance level was set at $p < 0.002$ following Bonferroni's correction. BCEA = bivariate contour ellipse area, BCVA = best-corrected visual acuity, CRT = central retinal thickness, EZ = ellipsoid zone, FST = full-field stimulus testing, MS = macular sensitivity on microperimetry, PR = photoreceptor layers, RPE = retinal pigment epithelium.

* Sensitivity at the central fixation point, as measured with microperimetry, which was the fovea in 17/39 eyes (44%), and an eccentric location in the other eyes.

** Patients with cystoid macular oedema, and therefore increased central retinal thickness, were not included in the analysis of correlations between central retinal thickness and visual function parameters.

clinical spectrum. We define parameters that are potentially the most appropriate clinical and surrogate end-points for a future *CRB1*-gene therapy trial, as well as risk factors for potential adverse treatment reactions. Complementary to time-dependant end-points, which may remain stable for years and which we investigated earlier in the largest retrospective longitudinal study to date, potential surrogate end-points were evaluated in this cross-sectional study through careful structure–function correlation analysis. Diagnoses included RP (86%), CORD (9%) and macular dystrophy (5%). Interfamilial variability and a degree of intrafamilial variability were observed on ophthalmoscopy and retinal imaging, with both adulthood-onset CORD and infancy-onset RP present in the same genetic isolate, in patients carrying the same homozygous mutation. Generally, interfamilial variability was greater than intrafamilial variability. There was a wide range of age at initial symptom onset, although half of RP patients reported this onset to be either in infancy or first years of life. Patients with a cone-rod or macular dystrophy had a later symptom onset, which follows some reports of *CRB1*-associated macular dystrophies that have a decidedly milder phenotype than *CRB1*-RP (Khan et al. 2018).

Contrasting the progressive nature of *CRB1*-associated disease in individual patients (Mathijssen et al. 2017; Talib et al. 2017), in this cross-sectional study we found lower visual acuities in younger patients. This counterintuitive finding may be a result of the inclusion criterion of a BCVA ≥ 0.05, which could result in a narrow and particularly early-in-life window for study inclusion in patients with severe early-onset RP, while posing a broader window for inclusion in patients with mild RP or CORD, who maintain a better BCVA into mid-adulthood. Our results show that despite the previously demonstrated intra-individual progressive visual deterioration (Mathijssen et al. 2017; Talib et al. 2017), at a cross-sectional population level no simple relationship is found between age and visual function parameters, such as BCVA and visual field area.

Spectral-domain optical coherence tomography (SD-OCT) revealed CME in 38% of patients in this cohort, which is a comparable number to earlier reports of CME in genetically diverse or undifferentiated RP cohorts (Hajali et al. 2008; Testa et al. 2014). Patients with CME in this cohort were on average 10 years younger and had a significantly better BCVA than those without CME, despite the trend for a lower BCVA in younger patients at a cross-sectional level. This suggests that CME is an early disease feature in *CRB1* retinopathy. Follow-up SD-OCTs in the same patients should reveal whether the CME reduces after an extended period of time and whether the macula is more strongly degenerated in areas of previous cystoid maculopathy. The aetiology for CME in RP is not fully clear. Müller cell dysfunction and oedema has been posed as a potential cause of CME (Reichenbach et al. 2007), which is supported by the location of the CME in the INL. Müller cells have already been shown to play an important role in the aetiology of *CRB1*-associated vascular abnormalities in mice and rats (van de Pavert et al. 2007; Zhao et al. 2015). Earlier fluorescein angiography in three cases of *CRB1* retinopathy has shown no leakage in patients with CME (Khan et al. 2014; Cordovez et al. 2015), in contrast with extensive leakage starting from the early phases in Coats-like exudative vasculopathy (Hasan et al. 2016), which is a recurring finding in *CRB1* retinopathies (van den Born et al. 1994; den Hollander et al. 2001). Our current findings of parapapillary hard exudates in a 41-year-old patient and a preretinal haemorrhage of unknown origin in a 10-year-old patient further point to a vascular component of *CRB1* retinopathies. The parapapillary hard exudates may be a precursor of Coats-like exudative vasculopathy, which the older and blind sibling of this patient had been diagnosed with, but SD-OCT of the optic disc revealed no source of the exudation. A preretinal haemorrhage as in the 10-year-old has been described in *CRB1*-retinopathies once before in two

affected sisters (aged 3 and 5) undergoing interventions in the alternative circuit involving the Valsalva manoeuvre and repeated intense pressure on the soft palate, where these haemorrhages were bilateral and self-limiting (Bifari & Khan 2016). Other findings on SD-OCT included thickening of the inner retina (95%), and coarsening (38%) or disorganization (38%) of the retinal laminar structure. Inner retinal thickening has been observed in human patients with *CRB1* retinopathy (Aleman et al. 2011), and has also been demonstrated in mice lacking CRB1 and CRB2 in retinal progenitor cells, in which the thickening was caused by a proliferation of retinal progenitors which resulted in an increase in the number of rod photoreceptors, Müller cells and bipolar cells (Pellissier et al. 2013). A recent mouse study showed a role for Crb2 in the thickening of the ganglion cell layer due to ectopic photoreceptors (Quinn et al. 2018). Some studies have shown a milder degree of inner retinal thickening in association with ONL thinning, for example in *RHO*- and *RPGR*-associated retinopathies (Aleman et al. 2007; Aleman et al. 2008). These studies have suggested that this inner retinal thickening may be due to a remodelling process and may precede eventual inner retinal atrophy (Aleman et al. 2007; Aleman et al. 2008). Retinal remodelling could possibly interfere with a functional (gene) therapeutic effect. However, in this cohort, inner retinal thickness was not associated with thinning of the outer retina and RPE, indicating that the cause for the inner retinal thickening is more likely the presence of ectopic photoreceptors, or Müller cell or bipolar cell proliferation, rather than remodelling.

In some cases, the *CRB1*-associated phenotype appears associated with the genotype. For instance, optic nerve head drusen or hamartomas were more prevalent in patients from the genetic isolate in our cohort ($p = 0.02$), confirming the findings in our previous retrospective study (Talib et al. 2017). Patients from the genetic isolate did not have significant differences in visual function with patients from outside the genetic isolate. Another genotype–phenotype correlation in this study involved the p.(Ile167_Gly169del) mutation, found in homozygous form in patient ID-22, who had an isolated maculopathy, and which has been reported before in most cases of isolated maculopathy, even in compound heterozygosity (Sánchez-Alcudia et al. 2014; Shah et al. 2016; Khan et al. 2018; Mucciolo et al. 2018). *CRB1*-associated maculopathy has also been reported in association with other mutations (Tsang et al. 2014; Wolfson et al. 2015). It should be noted that in our study, the p.(Tyr631Cys) mutation, which to our knowledge has not been described outside of this cohort, was observed in two patients with an unusually mild phenotype, characterized by preserved BCVA, a normal retinal laminar organization and preservation of outer retinal structures into the 4th and 8th decades of life. The p.(Pro836Thr) mutation was found in association with CORD in this study (patient 21; originally from the Caribbean), but has been reported before in association with early-onset retinal dystrophy in a Malinese patient (Bujakowska 2012). As genotype–phenotype correlations do not explain the contrasting phenotypic findings in this cohort or the intrafamilial phenotypic variability, there may be a role for genetic and/or environmental modifiers. Disruption of one allele or two alleles of *Crb2* has recently been shown to aggravate the *Crb1*-associated phenotype in mice (Quinn et al. 2018) and may be an avenue for further investigation.

Implications of this study for therapeutic interventions such as gene therapy include the assessment of the phenotype's amenability to treatment, identification of potential risk factors and the evaluation of structure–function correlations. The amenability of the *CRB1*-associated phenotype to treatment is supported by the variable degrees of EZ preservation on SD-OCT, and the (near-) normal laminar structure in 24% of patients, and laminar coarsening without disorganization in another 38% of patients. However, the visual deterioration in young patients, and the universal presence of macular RPE alterations or atrophy appears to suggest that intervention is desirable before the 3rd or 4th decades of life. Some retinas may have been weakened by the presence of CME, as is illustrated by the presence of lamellar pseudohole in one patient, and this may be a contra-indication for intervention using subretinal injection due to the risk of for instance macular hole formation. Generally, intra-ocular surgery in nanophthalmic eyes has been associated with a higher intra-operative and postoperative complication rate (Jung et al. 2012; Steijns et al. 2013), although no data have been published on the technical challenges in subretinal gene therapy surgery in nanophthalmic eyes. Appropriate pre-operative assessment and careful intra-operative measures should be taken in these high-risk eyes. A risk factor for complications in a future gene therapy trial is the narrow anterior chamber angle, as the associated risk of acute angle-closure glaucoma may be increased by repeated mydriasis and dark adaptation during a trial, as happened with patient ID-15 in this study. In clinical practice, biometry and assessment of the anterior chamber angle and intra-ocular pressure are useful in patients with *CRB1*-retinopathies, and at-risk patients should be instructed on alarm features. In the case of acute angle-closure glaucoma, prophylactic peripheral iridotomy in the contralateral eye may be indicated.

An important assumption in gene therapy trials where one eye is treated in each patient, and the nontreated eye is used as a control, is the symmetry and thus the comparability in visual function between eyes. We have found statistically significant intra-individual between-eye symmetry in all measures of visual function in our study, with a moderate degree of symmetry in BCVA, and very high degrees of symmetry in sensitivity thresholds on full-field stimulus testing and microperimetry, and in seeing retinal areas on Goldmann visual fields. Therefore, the nontreated contralateral eye is a suitable control in a future gene therapy trial for *CRB1*-associated RDs.

The most robust structure–function correlation, and the only statistically significant one after stringent correction for multiple testing, was the foveal PR + RPE thickness, as measured from the ELM to the basal membrane, to BCVA. The granular aspect of the hyperreflective outer retinal bands, including the EZ, complicated the evaluation of the EZ diameter and may explain why EZ diameter proved a less robust correlation with function parameters, such as BCVA and macular sensitivity. In other forms of RP, EZ diameter has been sensitive in

detecting disease progression (Cai et al. 2014; Cabral et al. 2017), and further prospective follow-up measurements are necessary to test this sensitivity in *CRB1* retinopathies. On the other hand, substantial photoreceptor populations have been demonstrated with adaptive optics in areas of low or no EZ reflectivity, indicating that biomarkers on SD-OCT do not always accurately represent photoreceptor cytology (Scoles et al. 2016). Prospective longitudinal measurements of the biomarkers on SD-OCT need to be correlated to visual function decline in *CRB1* retinopathies, in order to assess their potential as a surrogate endpoint in a future clinical gene therapy trial. Performing microperimetry was challenging in patients with severe visual impairment and could not be reliably performed in the two youngest patients. Inconveniently, these patients groups are of particular interest for microperimetric evaluation, as severely visually impaired patients (over the age of 18) will be the most likely to be included in a phase I trial. The shifting of the preferred retinal locus between the test run and the examination, which occurred in six patients, might pose a challenge in the second measurement for these patients. Prospective longitudinal measurements will decide whether this is correct and whether microperimetry offers a reliable functional outcome parameter. In this study, FST was successful in determining retinal sensitivity thresholds in patients with a wide range of vision loss and loss of electrophysiological responses. Full-field stimulus testing (FST) response to red stimuli at a lower intensity is mostly cone-mediated and would thus provide a method for measuring changes in cone sensitivity. A limitation of FST is its inability to localize the retinal area mediating the sensitivity threshold. In future subretinal gene therapy trials, this area may not co-localize with the location of the retinal area that was treated with subretinal injection of the treatment vector. Nonetheless, it has been sensitive in detecting sensitivity changes in gene therapy trials, while BCVA proved less sensitive (Bennett et al. 2016). Based on our findings, changes in FST would have to exceed the variability threshold of 4 dB in order to be reliably attributed to a therapeutic effect.

In conclusion, this prospective cross-sectional study provides extensive phenotypic characterization of *CRB1*-associated retinopathies, which are a candidate for gene therapy. Longitudinal prospective measurements of the same parameters are necessary in order to assess which outcome measures are the most sensitive in detecting the rate of progression and potential treatment effect in a future gene therapy trial.

References

Aleman TS, Cideciyan AV, Sumaroka A et al. (2007): Inner retinal abnormalities in X-linked retinitis pigmentosa with RPGR mutations. Invest Ophthalmol Vis Sci **48**: 4759–4765.

Aleman TS, Cideciyan AV, Sumaroka A et al. (2008): Retinal laminar architecture in human retinitis pigmentosa caused by Rhodopsin gene mutations. Invest Ophthalmol Vis Sci **49**: 1580–1590.

Aleman TS, Cideciyan AV, Aguirre GK et al. (2011): Human CRB1-associated retinal degeneration: comparison with the rd8 Crb1-mutant mouse model. Invest Ophthalmol Vis Sci **52**: 6898–6910.

Bennett J, Wellman J, Marshall KA et al. (2016): Safety and durability of effect of contralateral-eye administration of AAV2 gene therapy in patients with childhood-onset blindness caused by RPE65 mutations: a follow-on phase 1 trial. Lancet **388**: 661–672.

Bernal S, Calaf M, Garcia-Hoyos M, Garcia-Sandoval B, Rosell J, Adan A, Ayuso C & Baiget M (2003): Study of the involvement of the RGR, CRPB1, and CRB1 genes in the pathogenesis of autosomal recessive retinitis pigmentosa. J Med Genet **40**: e89.

Bifari IN & Khan AO (2016): Bilateral retinal hemorrhages following finger pressure against the soft palate () in recessive CRB1-related retinopathy. Ophthalmic Genet **37**: 441–444.

van den Born LI, van Soest S, van Schooneveld MJ, Riemslag FC, de Jong PT & Bleeker-Wagemakers EM (1994): Autosomal recessive retinitis pigmentosa with preserved para-arteriolar retinal pigment epithelium. Am J Ophthalmol **118**: 430–439.

Bujakowska K (2012): CRB1 mutations in inherited retinal dystrophies. Hum Mutat **33**: 306–315.

Cabral T, Sengillo JD, Duong JK et al. (2017): Retrospective analysis of structural disease progression in retinitis pigmentosa utilizing multimodal imaging. Sci Rep **7**: 10347.

Cai CX, Locke KG, Ramachandran R, Birch DG & Hood DC (2014): A comparison of progressive loss of the ellipsoid zone (EZ) band in autosomal dominant and x-linked retinitis pigmentosa. Invest Ophthalmol Vis Sci **55**: 7417–7422.

Collison FT, Fishman GA, McAnany JJ, Zernant J & Allikmets R (2014): Psychophysical measurement of rod and cone thresholds in stargardt disease with full-field stimuli. Retina **34**: 1888–1895.

Cordovez JA, Traboulsi EI, Capasso JE et al. (2015): Retinal dystrophy with intraretinal cystoid spaces associated with mutations in the crumbs homologue (CRB1) gene. Ophthalmic Genet **36**: 257–264.

Corton M, Tatu SD, Avila-Fernandez A et al. (2013): High frequency of CRB1 mutations as cause of Early-Onset Retinal Dystrophies in the Spanish population. Orphanet J Rare Dis **8**: 20.

Dagnelie G (1990): Conversion of planimetric visual field data into solid angles and retinal areas. Clin Vis Sci **5**: 95–100.

Ferris FL 3rd & Bailey I (1996): Standardizing the measurement of visual acuity for clinical research studies: Guidelines from the Eye Care Technology Forum. Ophthalmology **103**: 181–182.

Ferris FL 3rd, Kassoff A, Bresnick GH & Bailey I (1982): New visual acuity charts for clinical research. Am J Ophthalmol **94**: 91–96.

Galvin JA, Fishman GA, Stone EM & Koenekoop RK (2005): Evaluation of genotype-phenotype associations in leber congenital amaurosis. Retina **25**: 919–929.

Hajali M, Fishman GA & Anderson RJ (2008): The prevalence of cystoid macular oedema in retinitis pigmentosa patients determined by optical coherence tomography. Br J Ophthalmol **92**: 1065–1068.

Hasan SM, Azmeh A, Mostafa O & Megarbane A (2016): Coat's like vasculopathy in leber congenital amaurosis secondary to homozygous mutations in CRB1: a case report and discussion of the management options. BMC Res Notes **9**: 91.

Hettinga YM, van Genderen MM, Wieringa W, Ossewaarde-van Norel J & de Boer JH (2016): Retinal dystrophy in 6 young patients who presented with intermediate uveitis. Ophthalmology **123**: 2043–2046.

den Hollander AI, ten Brink JB, de Kok YJ et al. (1999): Mutations in a human homologue of Drosophila crumbs cause retinitis pigmentosa (RP12). Nat Genet **23**: 217–221.

den Hollander AI, Heckenlively JR, van den Born LI et al. (2001): Leber congenital amaurosis and retinitis pigmentosa with Coats-like exudative vasculopathy are associated with mutations in the crumbs homologue 1 (CRB1) gene. Am J Hum Genet **69**: 198–203.

van Huet RA, Oomen CJ, Plomp AS et al. (2014): The RD5000 database: facilitating clinical, genetic, and therapeutic studies on inherited retinal diseases. Invest Ophthalmol Vis Sci **55**: 7355–7360.

van Huet RA, Siemiatkowska AM, Ozgul RK et al. (2015): Retinitis pigmentosa caused by mutations in the ciliary MAK gene is relatively mild and is not associated with apparent extra-ocular features. Acta Ophthalmol **93**: 83–94.

Jalkh N, Guissart C, Chouery E, Yammine T, El Ali N, Farah HA & Megarbane A (2014): Report of a novel mutation in CRB1 in a Lebanese family presenting retinal dystrophy. Ophthalmic Genet **35**: 57–62.

Jung KI, Yang JW, Lee YC & Kim SY (2012): Cataract surgery in eyes with nanophthalmos and relative anterior microphthalmos. Am J Ophthalmol **153**: 1161–1168.e1161.

Khan AO, Aldahmesh MA, Abu-Safieh L & Alkuraya FS (2014): Childhood cone-rod dystrophy with macular cystic degeneration from recessive CRB1 mutation. Ophthalmic Genet **35**: 130–137.

Khan KN, Robson A, Mahroo OAR et al. (2018): A clinical and molecular characterisation of CRB1-associated maculopathy. Eur J Hum Genet **26**: 687–694.

Klein M & Birch DG (2009): Psychophysical assessment of low visual function in patients with retinal degenerative diseases (RDDs) with the Diagnosys full-field stimulus threshold (D-FST). Doc Ophthalmol **119**: 217–224.

Koenekoop RK, Sui R, Sallum J et al. (2014): Oral 9-cis retinoid for childhood blindness due to Leber congenital amaurosis caused by RPE65 or LRAT mutations: an open-label phase 1b trial. Lancet **384**: 1513–1520.

Lotery AJ, Jacobson SG, Fishman GA et al. (2001a): Mutations in the CRB1 gene cause Leber congenital amaurosis. Arch Ophthalmol **119**: 415–420.

Lotery AJ, Malik A, Shami SA et al. (2001b): CRB1 mutations may result in retinitis pigmentosa without para-arteriolar RPE preservation. Ophthalmic Genet **22**: 163–169.

Mathijssen IB, Florijn RJ, van den Born LI et al. (2017): Long-term follow-up of patients with retinitis pigmentosa type 12 caused by CRB1 mutations: a severe phenotype with considerable interindividual variability. Retina **37**: 161–172.

McCulloch DL, Marmor MF, Brigell MG, Hamilton R, Holder GE, Tzekov R & Bach M (2015): ISCEV Standard for full-field clinical electroretinography (2015 update). Doc Ophthalmol **130**: 1–12.

McKibbin M, Ali M, Mohamed MD et al. (2010): Genotype-phenotype correlation for leber congenital amaurosis in Northern Pakistan. Arch Ophthalmol **128**: 107–113.

Morarji J, Lenassi E, Black GC & Ashworth JL (2016): Atypical presentation of CRB1 retinopathy. Acta Ophthalmol. **94**: e513–e514.

Mucciolo DP, Murro V, Giorgio D, Passerini I, Sodi A, Virgili G & Rizzo S (2018): Long-term follow-up of a CRB1-associated maculopathy. Ophthalmic Genet, **39**(4), 522–525.

van de Pavert SA, Kantardzhieva A, Malysheva A et al. (2004): Crumbs homologue 1 is required for maintenance of photoreceptor cell polarization and adhesion during light exposure. J Cell Sci **117**: 4169–4177.

van de Pavert SA, Sanz AS, Aartsen WM et al. (2007): Crb1 is a determinant of retinal apical Muller glia cell features. Glia **55**: 1486–1497.

Pellissier LP, Alves CH, Quinn PM et al. (2013): Targeted ablation of CRB1 and CRB2 in retinal progenitor cells mimics Leber congenital amaurosis. PLoS Genet **9**: e1003976.

Pellissier LP, Quinn PM, Alves CH, Vos RM, Klooster J, Flannery JG, Heimel JA & Wijnholds J (2015): Gene therapy into photoreceptors and Muller glial cells restores retinal structure and function in CRB1 retinitis pigmentosa mouse models. Hum Mol Genet **24**: 3104–3118.

Quinn PM, Pellissier LP & Wijnholds J (2017): The CRB1 complex: following the trail of crumbs to a feasible gene therapy strategy. Front Neurosci **11**: 175.

Quinn PM, Alves CH, Klooster J & Wijnholds J (2018): CRB2 in immature photoreceptors determines the superior-inferior symmetry of the developing retina to maintain retinal structure and function. Hum Mol Genet **27**: 3137–3153.

Reichenbach A, Wurm A, Pannicke T, Iandiev I, Wiedemann P & Bringmann A (2007): Muller cells as players in retinal degeneration and edema. Graefes Arch Clin Exp Ophthalmol **245**: 627–636.

Roman AJ, Schwartz SB, Aleman TS et al. (2005): Quantifying rod photoreceptor-mediated vision in retinal degenerations: dark-adapted thresholds as outcome measures. Exp Eye Res **80**: 259–272.

Roman AJ, Cideciyan AV, Aleman TS & Jacobson SG (2007): Full-field stimulus testing (FST) to quantify visual perception in severely blind candidates for treatment trials. Physiol Meas **28**: N51–56.

Sánchez-Alcudia R, Cortón M, Ávila-Fernández A et al. (2014): Contribution of mutation load to the intrafamilial genetic heterogeneity in a large cohort of spanish retinal dystrophies families. Invest Ophthalmol Vis Sci **55**: 7562–7571.

Scoles D, Flatter JA, Cooper RF et al. (2016): Assessing photoreceptor structure associated with ellipsoid zone disruptions visualized with optical coherence tomography. Retina **36**: 91–103.

Shah N, Damani MR, Zhu XS, Bedoukian EC, Bennett J, Maguire AM & Leroy BP (2016): Isolated maculopathy associated with biallelic CRB1 mutations. Ophthalmic Genet, **38**(2), 190–193.

Steijns D, Bijlsma WR & Van der Lelij A (2013): Cataract surgery in patients with nanophthalmos. Ophthalmology **120**: 266–270.

Talib M, van Schooneveld MJ, van Genderen MM et al. (2017): Genotypic and phenotypic characteristics of CRB1-associated retinal dystrophies: a long-term follow-up study. Ophthalmology **124**: 884–895.

Testa F, Rossi S, Colucci R et al. (2014): Macular abnormalities in Italian patients with retinitis pigmentosa. Br J Ophthalmol **98**: 946–950.

Tsang SH, Burke T, Oll M, Yzer S, Lee W, Xie YA & Allikmets R (2014): Whole exome sequencing identifies CRB1 defect in an unusual maculopathy phenotype. Ophthalmology **121**: 1773–1782.

Vallespin E, Cantalapiedra D, Riveiro-Alvarez R et al. (2007): Mutation screening of 299 Spanish families with retinal dystrophies by Leber congenital amaurosis genotyping microarray. Invest Ophthalmol Vis Sci **48**: 5653–5661.

Vincent A, Ng J, Gerth-Kahlert C et al. (2016): Biallelic mutations in CRB1 underlie autosomal recessive familial foveal retinoschisis. Invest Ophthalmol Vis Sci **57**: 2637–2646.

Wolfson Y, Applegate CD, Strauss RW, Han IC & Scholl HP (2015): CRB1-related maculopathy with cystoid macular edema. JAMA Ophthalmol **133**: 1357–1360.

Yang L, Wu L, Yin X, Chen N, Li G & Ma Z (2014): Novel mutations of CRB1 in Chinese families presenting with retinal dystrophies. Mol Vis **20**: 359–367.

Zhao M, Andrieu-Soler C, Kowalczuk L et al. (2015): A New CRB1 rat mutation links müller glial cells to retinal telangiectasia. J Neurosci **35**: 6093–6106.

Received on March 5th, 2019.
Accepted on July 21st, 2020.

Correspondence:
Camiel J.F. Boon, MD, PhD
Department of Ophthalmology
The Leiden University Medical Center
Postal zone J3-S
2333 ZA Leiden
Zuid-Holland
The Netherlands
Tel: +31(0)71 526 2388
Fax: +31(0)71 524 8222
Email: c.j.f.boon@lumc.nl

This work was supported by the Curing Retinal Blindness Foundation (Ivyland, PA, USA), Stichting Blindenhulp (The Netherlands), Janivo Stichting (The Netherlands) and Bayer Ophthalmology Research Award (The Netherlands). The Leiden University Medical Center (LUMC) is the holder of patent application PCT/NL2014/050549, which describes the potential clinical use of CRB2; JW is listed as inventor on this patent, and JW is an employee of the LUMC.

The authors wish to acknowledge dr. Y.Y. Cheng (LUMC) for reviewing the corneal topography results.

All authors attest that they meet the current ICMJE criteria for authorship.

Supporting Information

Additional Supporting Information may be found in the online version of this article:

Fig. S1 Flowchart showing the patient outreach and inclusion process.
Fig. S2 Evaluation of laminar organization and retinal architecture on spectral domain optical coherence tomography (SD-OCT) in patients with *CRB1*-associated retinal dystrophy.
Fig. S3 Scatterplots of between-eye symmetry of visual function in patients with *CRB1*-associated retinal dystrophies.
Fig. S4 Quantitative analysis of biomakers on spectral domain optical coherence tomography in *CRB1*-retinopathies.
Table S1 CRB1 mutations in this study.
Table S2 Retinal sensitivity measurements in *CRB1*-associated retinal dystrophies.
Table S3 Treatment histories for cystoid macular edema in CRB1-associated retinopathies.